Polymer 103 (2016) 152–162

Contents lists available at ScienceDirect

Polymer

journal homepage: www.elsevier.com/locate/polymer

Cross-link inhomogeneity in phenolic resins at the initial stage of curing studied by ^{1}H-pulse NMR spectroscopy and complementary SAXS/WAXS and SANS/WANS with a solvent-swelling technique

Atsushi Izumi [a, *], Yasuyuki Shudo [a, b], Toshio Nakao [b], Mitsuhiro Shibayama [b, **]

[a] Corporate R&D Center, Sumitomo Bakelite Co., Ltd., 1-1-5 Murotani, Nishi-ku, Kobe, Hyogo, 651-2241, Japan
[b] Neutron Science Laboratory, Institute for Solid State Physics, The University of Tokyo, 5-1-5 Kashiwanoha, Kashiwa, Chiba, 277-8581, Japan

ARTICLE INFO

Article history:
Received 16 June 2016
Received in revised form
25 August 2016
Accepted 19 September 2016
Available online 20 September 2016

Keywords:
Phenolic resins
Cross-link inhomogeneity
Curing process

ABSTRACT

The cross-link inhomogeneity of phenolic resins at the initial stage of curing in a temperature range of 110–130 °C was investigated through structural analysis of the network structure evolution mechanism using ^{1}H-pulse nuclear magnetic resonance spectroscopy and complementary small- and wide-angle X-ray and neutron scattering methods. Two types of phenolic resins, PR06 and PR12, were prepared with stoichiometrically insufficient and sufficient amounts of cross-linker, respectively, via curing of a novolac-type phenolic resin oligomer with hexamethylenetetramine as the curing agent. Their network structures comprised three different structural domains because of the cross-link inhomogeneity: the high-cross-link-density domain (HXD), the low-cross-link-density domain (LXD), and the interface region between these domains. Percolation of the HXD occurred at the beginning of the curing. Intradomain reactions inside both HXD and LXD proceeded as the dominant reactions accompanying minor interdomain reactions between the HXDs, resulting in no significant change in the spatial location and size of the HXDs and LXDs. Intradomain reactions inside the LXD involved reactions with dangling chains, which would not affect the average mesh size of the domain significantly. These behaviors of the network structure evolution mechanism at the initial stage of the curing are a general feature of phenolic resins that does not depend on the amount of cross-linker. The difference between the amount of the cross-linker present in PR06 and PR12 was manifested as a difference in the degree of cross-linking in the percolated HXDs, i.e., the HXD of PR12 exhibited a tightly cross-linked, well-developed network structure since the beginning of the curing process; however, that of PR06 exhibited a loosely cross-linked network structure, with the degree of cross-linking increasing as the curing proceeded.

1. Introduction

Phenolic resins were the first example of artificial plastics based on a synthetic polymer and were invented by Baekeland in 1907. Because of their excellent mechanical and electrical properties as well as their heat and solvent resistance, they have been employed as insoluble and infusible thermosetting resins in electronics, the automotive industry, housing, and other general industries, and the application has now extended to the space industry [1,2]. These crucial properties are provided by a three-dimensional cross-linked network structure that comprises phenols and methylenes as represented in a two-dimensional manner in Fig. 1. This structure is typically obtained by the curing of a novolac-type phenolic resin oligomer with hexamethylenetetramine (HMTA) as a curing agent, wherein HMTA decomposes to methylene cross-linkers with emitting ammonia gas [1].

It is believed that fully cured phenolic resins inevitably exhibit cross-link inhomogeneity in their network structure and this inhomogeneity strongly influences their abovementioned desirable properties; however, details of the cross-link inhomogeneity have not yet been fully elucidated owing to the difficulty in structural analysis of fully cured resins, which arises from their insolubility, infusibility, and non-crystallinity. Thus, elucidation of the cross-link inhomogeneity to characterize their structure–property relations has been a major challenge for the structural analysis of phenolic

* Corresponding author.
** Corresponding author.
E-mail addresses: atsushi_i@sumibe.co.jp (A. Izumi), sibayama@issp.u-tokyo.ac.jp (M. Shibayama).

http://dx.doi.org/10.1016/j.polymer.2016.09.067
0032-3861/

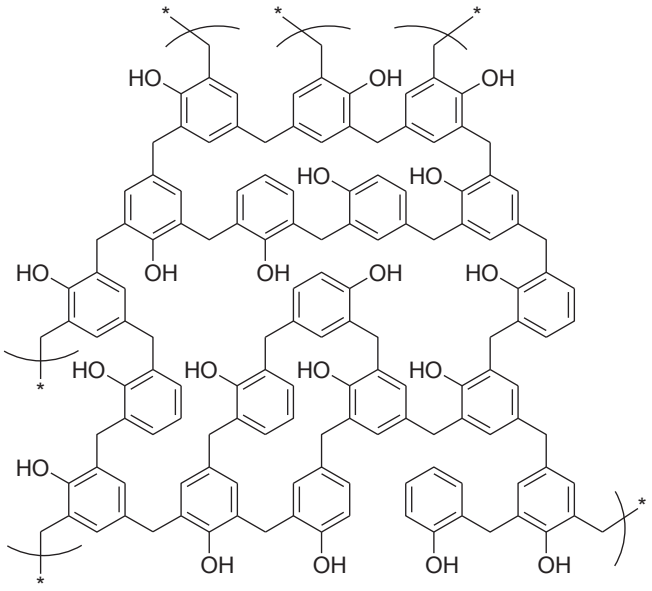

Fig. 1. Chemical structure of a cross-linked phenolic resin.

and other thermosetting resins for over a century [3–11].

This study focuses on understanding the inhomogeneity of phenolic resins using nuclear magnetic resonance (NMR) spectroscopy and light, X-ray, and neutron scattering analyses of (I) the oligomerization process at the pre-gelation stage [12], (II) the gelation process near the gel point [13,14], and (III) the fully cured stage [15,16]. The gel point is defined as the point at which an insoluble fraction in a suitable solvent is first detected. During the pre-gelation stage (I), the polymers exhibit a self-similar structure with respect to molecular weight distribution, which is irrespective of polycondensation conditions of phenol and formaldehyde, and no indication of inhomogeneity is observed. Conversely, the inhomogeneity appears near the gel point (II) because of gelation mechanisms that depend on the amount of cross-linker, which was characterized by precise analysis of the phenol–formaldehyde polycondensation system under a constant reaction temperature of 100 °C. For a stoichiometrically insufficient amount of cross-linker, inhomogeneous domains with a loosely cross-linked network appear at the gel point, and the intradomain reactions become dominant with an increase in the degree of cross-linking in the domain, whereas for a stoichiometrically sufficient amount of cross-linker, inhomogeneous domains with a tightly cross-linked network appear at the gel point and the interdomain reactions between the inhomogeneous domains become dominant with an increase in the size of the domain. However, the cross-link inhomogeneity observed in the gelation process near the gel point has not been observed in the fully cured stage (III) for the phenolic resins cured at 175 °C with different amounts of HMTA as the curing agent. Therefore, we have concluded that the elucidation of the network structure evolution mechanism in the post-gelation stage between stages (II) and (III), i.e., at the initial stage of the curing process beyond the gel point, is also important for elucidating the inhomogeneity in fully cured phenolic resins.

In our previous study, we demonstrated that ^{1}H-pulse NMR spectroscopy and small- and wide-angle X-ray scattering (SAXS and WAXS, respectively) in conjunction with a solvent-swelling technique are promising methods for elucidating the cross-link inhomogeneity in phenolic resins during the gelation process near the gel point when their network structures are not developed properly [14]. ^{1}H-pulse NMR spectroscopy can provide information about the dynamics of the molecular mobility of polymer segments in the network structure [17–20]. These dynamics are related to the nuclear spin–spin relaxation behavior, also referred to as transverse relaxation decay, of the attached protons on applying a specific external magnetic field. Using this technique, the relaxation behavior can be studied as a change in macroscopic magnetization of the protons, where a lower molecular mobility corresponds to a shorter the relaxation time and vice versa. In cross-linked polymers, the molecular mobility of the polymer segments strongly depends on their local cross-link density, i.e., the mobility of the polymer segments in a high-cross-link-density domain (HXD) with a small mesh size is lower than that in a low-cross-link-density domain (LXD) with a large mesh size [21]. X-ray and neutron scattering have also proven to be powerful techniques for elucidating the cross-link inhomogeneity of polymer gel networks [22–26]. These scattering techniques reveal nanometer-scale structural details of a material by exploiting scattering length density fluctuations of electron and atomic nuclei therein, which scatter X-rays and neutrons, respectively. The use of both these scattering techniques can provide complementary information about a material because of the differences in the scattering phenomena. In most studies of polymer gels, the NMR and scattering methods use the swelling features of the gel because swelling enhances the local fluctuations in the cross-link density, resulting in large contrasts in the dynamics and scattering length density; that is, the solvent-swollen polymer gels are more informative than those in the bulk state for NMR and scattering analyses of the cross-link inhomogeneity.

The present study focuses on further elucidation of the cross-link inhomogeneity in phenolic resins at the initial stage of curing process beyond the gel point by investigating the network structure evolution mechanism in a temperature range of 110–130 °C through structural analysis of the HMTA-curing system using ^{1}H-pulse NMR spectroscopy, SAXS/WAXS, and small- and wide-angle neutron scattering (SANS and WANS, respectively) in conjunction with the solvent-swelling technique.

2. Experimental

2.1. Materials

A novolac-type phenolic resin oligomer (NV) with polystyrene-based weight- and number-average molecular weights of 3400 and 870 g mol^{-1}, respectively, was provided by Sumitomo Bakelite Co., Ltd. (Japan). HMTA was purchased from Chang Chun Petrochemical Co., Ltd. (Taiwan). Methanol (MeOH) and methanol-d_4 (MeOH-d_4) with a 99.8% degree of deuteration were purchased from Wako Pure Chemical Industries, Ltd. (Japan). All materials were used without further purification.

Curing reactions of NV with HMTA were performed using NV/HMTA weight ratios of 1/0.06 (PR06) and 1/0.12 (PR12), representing curing systems with stoichiometrically insufficient and sufficient amounts of cross-linker, respectively. It should be noted that the equivalent stoichiometric ratio in this curing system is 1/0.138 (wt/wt) based on the number-average molecular weight of NV, assuming NV to be a linear polymer with no branching structure. A mixture of NV/HMTA (50 g) was heated to melting at 100 °C under a pressure of 45 kPa for 5 h in a disk-shaped mold, then the resulting disk-shaped resin was milled and powdered at room temperature. Fig. 2 shows a differential scanning calorimetry (DSC) thermogram of the powdered PR12 that was recorded on a DSC-6220 (Seiko Instruments Inc., Japan) at a heating rate of 5 °C min^{-1}. The DSC result shows that the mixture has one broad exothermic region owing to cross-linking reactions, for which the

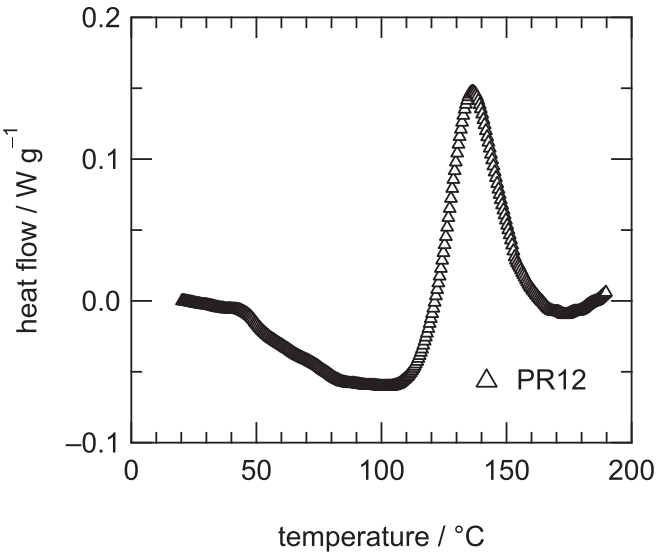

Fig. 2. DSC thermogram of PR12 prepared at 100 °C.

onset temperature is 110 °C and the peak is at 136 °C. Based on the DSC result, curing reactions of PR06 and PR12 were performed in the range 110–130 °C to investigate behavior at the initial stage of the curing process. The procedure for the curing reaction was as follows. The powdered sample was heated at 110 °C under 45 kPa for 5 h in the mold. The resulted resin was milled and powdered. A 5-g sample was then collected for analysis, and the rest of the powder was subjected to further curing. This heating-and-milling procedure was repeated stepwise in +5 °C increments to promote further reaction until 130 °C. Here the reaction time of 5 h was chosen to complete the reaction at the respective temperature under molding pressure.

A 2-g sample of the powder obtained at each temperature was stirred in a large amount of MeOH to extract the MeOH-soluble components, followed by centrifugation and collection of the MeOH-insoluble gels. This procedure was repeated three times, and the MeOH-insoluble gels were obtained in a fully MeOH-swollen state. It should be noted that there are many good solvents for phenolic resins such as tetrahydrofuran, MeOH, and acetone; however, methanol was chosen in this study because of the better solubility of HMTA.

2.2. Gel fraction

The gel fraction was calculated as the weight ratio of the MeOH-insoluble component of the 2-g powder sample, which was estimated from the weight of the MeOH-soluble component obtained by drying the combined extracts in vacuum.

2.3. Degree of swelling of the gel

Degree of swelling of the MeOH-insoluble gel (D_{swell}) was calculated as the volume ratio VV_0^{-1}, where V and V_0 denote the sample volumes before and after drying the fully MeOH-swollen gel, respectively. The sample volumes were estimated from their weights and densities, in which the densities of the MeOH and the phenolic resins were approximated to be 0.79 and 1.25 g mol^{-1}, respectively. The value of D_{swell} was obtained as the average of three measurements.

2.4. ^{1}H-pulse NMR spectroscopy

The ^{1}H-pulse NMR experiments were performed using an MQC23 benchtop NMR analyzer (Oxford Instruments plc, United Kingdom) with a 10-mm-diameter probe operated at 23 MHz. The MeOH-d_4-swollen phenolic resins were used as specimens to observe only the NMR signals of protons in the phenolic resins. Glass NMR tubes with a diameter of 10 mm and a wall thickness of 0.6 mm (JEOL RESONANCE Inc., Japan) were used for the sample cells. The spin–spin relaxation decay was recorded at 40 °C using Carr–Purcell–Meiboom–Gill pulse sequences. The pulse width, pulse interval (τ), number of ($180° - 2\tau$)-loops, relaxation delay between subsequent scans, and number of scans were set to 2.0 μs, 50 μs, 4096, 10 s, and 128, respectively.

2.5. SAXS and WAXS

SAXS measurements over a q range of 0.02–7 nm^{-1} were performed on a BL03XU beamline, which is known as the Frontier Softmaterial Beamline (FSBL), at SPring-8, Hyogo, Japan [27,28]. Here, q denotes the magnitude of the scattering vector given by $q = (4\pi\ \lambda^{-1})$ sin $(2\theta/2)$, where λ and 2θ denote the wavelength of the incident beam and the scattering angle, respectively. The measurements were performed at a sample-to-detector distance (SDD) of 3.4 m with a λ of 0.15 nm under vacuum using a windowless SAXS setup, and at an SDD of 1.2 m with a λ of 0.10 nm in air. The windowless SAXS setup was applied to achieve a higher signal-to-background scattering ratio by reducing background air scattering. The scattered X-rays were counted by an R-AXIS VII imaging plate detector system (Rigaku Corporation, Japan) with a 3000 × 3000 pixel array and a pixel size of 0.1 mm pixel^{-1}. WAXS measurements over a q range of 5.0–20 nm^{-1} were performed on a NANO-Viewer (Rigaku Corporation, Japan) using an X-ray beam with a λ of 0.154 nm from a CuKα spectral line excited at 40 kV and 30 mA. The scattered X-rays were counted by a Pilatus 100K detector system (DECTRIS Ltd., Switzerland) with a 487 × 195 pixel array and a pixel size of 0.172 mm pixel^{-1} at an SDD of 76 mm. Quartz glass capillaries Mark-Tube (Hilgenburg GmbH, Germany) with a diameter of 2 mm and a wall thickness of 0.01 mm were used as sample cells. The open top of the glass capillary was sealed using the silylated polyurethane adhesive (Konishi Co., Ltd., Japan) in order to place the MeOH-containing capillaries in the vacuum chamber. After correction for dark noise from the R-AXIS detector and defective pixels of the Pilatus detector, the transmittance, and background scattering, the scattering intensity was normalized to an absolute intensity scale with units of cm^{-1} using a 1-mm-thick glassy carbon plate (glassy carbon Type 2, Alfa Aesar, USA) as a secondary standard to combine the SAXS and WAXS data. The absolute scattering intensity function of the glassy carbon plate was determined using a previously calibrated glassy carbon plate [29].

2.6. SANS and WANS

SANS and WANS measurements over a q range of 0.08–170 nm^{-1} were performed on the BL15 beamline, which is known as "TAIKAN," installed in the Materials and Life Science Experimental Facility (MLF) of J-PARC, Tokai, Ibaraki, Japan. The MeOH-d_4-swollen phenolic resins were used instead of the MeOH-swollen phenolic resins to increase the coherent neutron scattering contrast between the phenolic resins and the solvent, and to reduce neutron incoherent scattering background noise from the solvent, which result from large differences in the coherent neutron scattering length and the incoherent neutron scattering cross section between ^{1}H and ^{2}H, respectively [30]. Sealable 2-mm-thick rectangular quartz cells (MITORIKA Co., Ltd. (formerly Mitorika Glass

Co., Ltd.), Japan) with a width and height of 22 and 45 mm, respectively, and a glass thickness of 1.0 mm were used as sample cells. A 10-mmφ neutron beam with a λ of 0.05–0.78 nm was used for measurement, and scattered neutrons were counted by a time-of-flight method using ^{3}He-position sensitive detectors mounted at four detector banks, i.e., small-, middle-, and high-angle banks, and a backward bank. The obtained two-dimensional scattering data were converted to one-dimensional data using a beamline specific data reduction program, in which the scattering data with a λ of 0.07–0.76 nm was used for the data reduction. The one-dimensional data obtained have a very wide q range of 0.08–170 nm^{-1}; however, the scattering data with $q > 30$ nm^{-1} was not used for further investigation in this study because an additional correction for inelastic neutron scattering is required for data in that range. The details of the instrument, data acquisition, and data reduction procedures are described in the literature [31].

3. Results and discussion

3.1. Gel fraction and degree of swelling

To understand the network structure evolution mechanism at the initial stage of the curing process from the macroscopic viewpoint, the MeOH-insoluble gel fraction in the cured phenolic resins and its degree of swelling in MeOH were first investigated. Fig. 3 shows the change in the gel fraction as a function of curing temperature. The gel fractions of PR06 and PR12 exceed 0.6 and 0.7, respectively, at 110 °C, and show a slight increase with curing temperature, which clearly indicates that the phenolic resins are well beyond the gel point. The progress of the cross-linking reaction beyond the gel point at 110 °C seems to be in contradiction to the DSC result shown in Fig. 2; however, this could be explained by the effect of the molding pressure, which accelerates the reaction in the mold.

Fig. 4 shows the change in D_{swell} as a function of curing temperature, which was calculated as a ratio of the volume change. The value D_{swell} for PR06 gradually decreases from 4.2 to 2.8 with curing temperature, whereas that for PR12 remains approximately constant at ca. 2.0. The values 4.2–2.8 and 2.0 correspond to swelling ratios of the length change of 1.6–1.4 and 1.3 assuming isotropic swelling. A decrease in D_{swell} can be generally explained by a

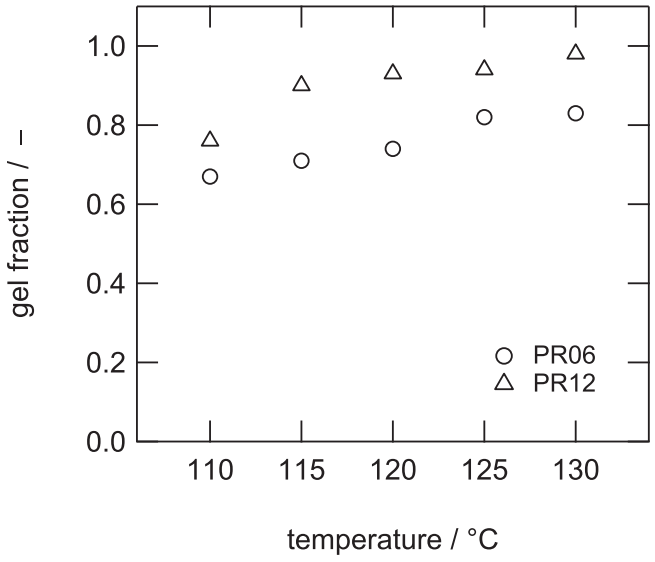

Fig. 3. Change in the MeOH-insoluble gel fraction: circles, PR06; and triangles, PR12.

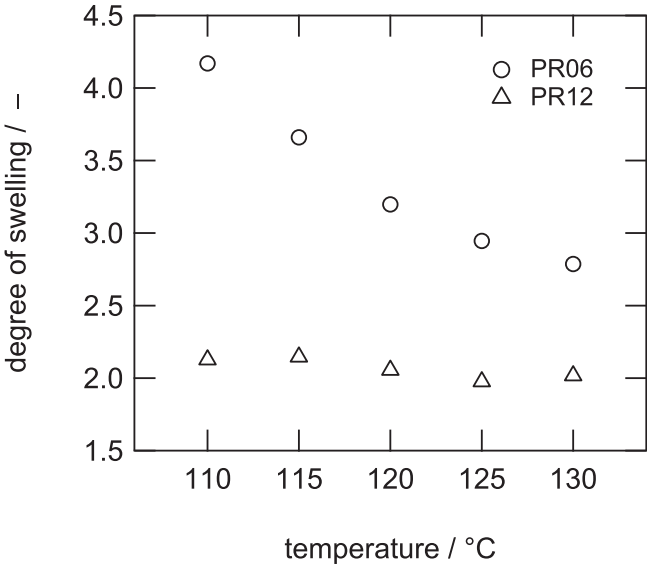

Fig. 4. Change in the degree of gel swelling in MeOH: circles, PR06; and triangles, PR12.

decrease in the average mesh size of the cross-linked network structure owing to an increase in the degree of cross-linking [32]; however, another mechanism should be considered for PR12, which exhibits a constant D_{swell}. A possible network structure evolution mechanism that results in the behavior of PR12 is that there are high- and low-cross-link-density domains (HXDs and LXDs, respectively) owing to the cross-link inhomogeneity and percolation of the HXD occurs at 110 °C. The percolated domains dominate the degree of swelling of the gel, in which the degree of swelling of the domain is 2.0. Consistent with this conjecture, PR06 may also exhibit percolation of the HXD that dominates the degree of swelling of the gel. In this case, the decrease in D_{swell} could be explained by assuming that the degree of cross-linking in the HXD of PR06 is lower than that in PR12, and the degree of cross-linking gradually increases with curing; that is, the well-developed, tightly cross-linked network structure results in a constant value for D_{swell} irrespective of the curing temperature, whereas the degree of cross-linking in the loosely cross-linked network structure increases via intradomain reactions accompanying a decrease in D_{swell} with the curing temperature. Here, the presence of tightly and loosely cross-linked network structures in the HXD could be explained by different gelation mechanisms near the gel point, which depend on the stoichiometric amount of cross-linker [14]. To investigate the mechanisms of the network structure evolution of PR06 and PR12 more precisely, a ^{1}H-pulse NMR analysis and complementary X-ray and neutron scattering analyses have been performed in the following subsections.

3.2. ^{1}H-pulse NMR

The nuclear spin–spin relaxation time function of protons is generally described by

$$M(t)/M(0) = \exp\left[-(1/a)\cdot(t/T_2)^a\right], \quad (1)$$

where t, $M(t)/M(0)$, a, and T_2 denote the decay time, normalized magnetization intensity at t, exponent of the decay function, and time constant representing the nuclear spin–spin relaxation of protons, respectively [17–19]. The value a ranges from 1 for an exponential-type slow decay to 2 for a Gaussian-type fast decay.

When the molecular mobility of the polymer segments is less constrained, such as in the rubbery and solution states, the relaxation function typically follows exponential-type slow decay. Conversely, when the mobility is highly constrained, such as in the glassy and crystalline states, the function typically follows Gaussian-type fast decay. Our previous study demonstrated that the molecular mobility of solvent-swollen phenolic resins having cross-link inhomogeneity can be classified into three relaxation modes with the value a of 1, and the spin–spin relaxation function can be expressed with a triple-exponential function given by

$$M(t)/M(0) = \phi_1 \exp(-t/T_{2,1}) + \phi_2 \exp(-t/T_{2,2}) + \phi_3 \exp(-t/T_{2,3}), \quad (2)$$

where φ_i and $T_{2,i}$ with $i = 1$, 2, and 3 denote the molar fraction of protons and time constant T_2 in the polymer segments of the i-th relaxation mode, respectively, in which the function was derived by a distribution analysis of T_2. Here, $\varphi_1 + \varphi_2 + \varphi_3 = 1$ and $T_{2,1} < T_{2,2} < T_{2,3}$. The first relaxation mode results from the spin–-spin relaxations of protons in polymer segments in the HXD where molecular mobility is highly constrained by the cross-links. The third relaxation mode results from the relaxations in the LXD where molecular mobility is less constrained. The second relaxation mode results from the relaxation at the interface region between the HXD and LXD [14].

Fig. 5 shows the spin–spin relaxation decay of PR06 and PR12 in the fully-MeOH-d_4 swollen state, in which solid lines are the fitting curves using Equation (2). The decay occurs faster with increased curing temperature, which clearly suggests a decrease in the average mesh size of the cross-linked network structure owing to the progress of curing.

Fig. 6a shows the fitting parameters $T_{2,1}$, $T_{2,2}$, and $T_{2,3}$ as a function of curing temperature with a logarithmic scale on the vertical axis, and Fig. 6b shows a re-plot of $T_{2,3}$ with a linear scale on the vertical axis. All the spin–spin relaxation decays shown in Fig. 5 clearly exhibit three different relaxation modes with time constants

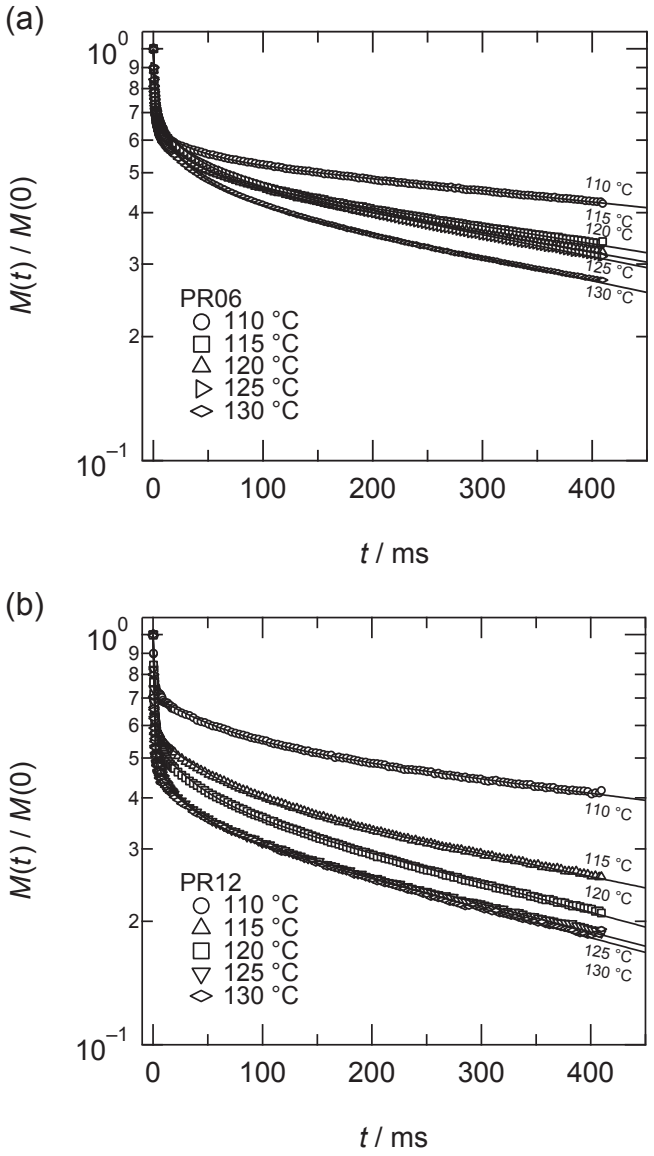

Fig. 5. Proton nuclear spin–spin relaxation decay in MeOH-d_4: (a) PR06 and (b) PR12.

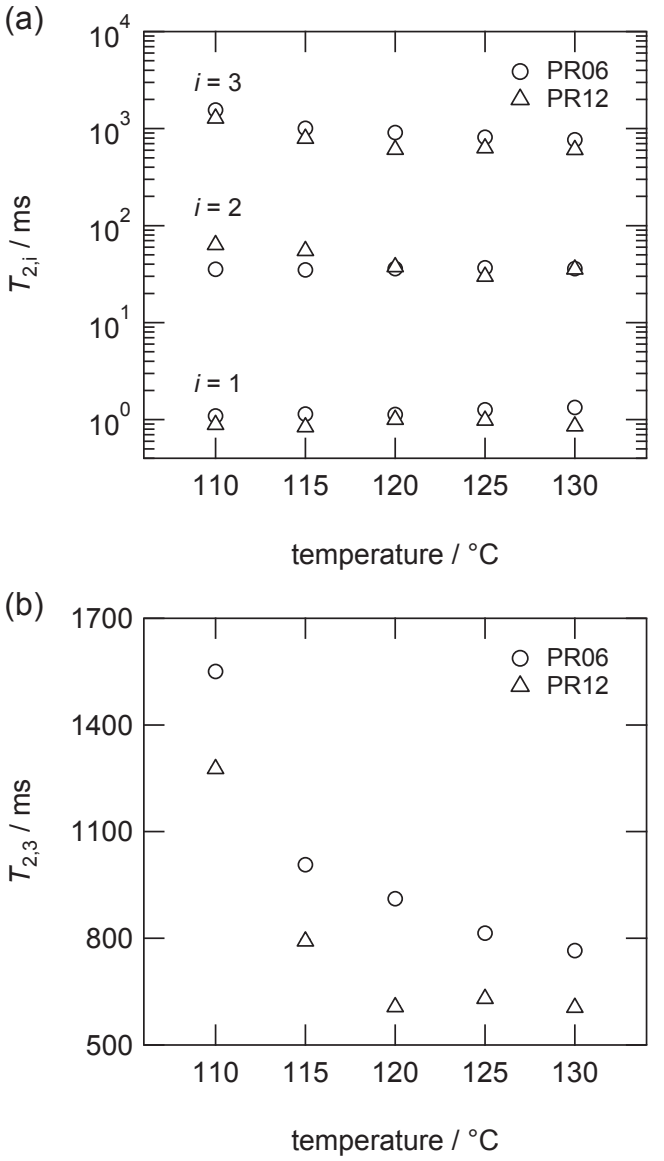

Fig. 6. (a) Change in $T_{2,n}$ (n = 1, 2, and 3) and (b) $T_{2,3}$ as a function of curing temperature: circles, PR06; and triangles, PR12. (b) Re-plot of $T_{2,3}$ as a function of curing temperature in a linear scale on the vertical axis.

in the orders of magnitude of 10^0, 10^1, and 10^2–10^3 ms, which are associated with the first, second, and third relaxation modes, respectively. As seen in Fig. 6a, PR06 and PR12 exhibit almost the same values of $T_{2,1}$ and $T_{2,2}$, which suggests that they have essentially the same mesh size in the HXD and the interface region. This seems to contradict the conjecture in the previous subsection that the degree of cross-linking in the HXD of PR06 is lower than that of PR12; however, the mesh size may be too small to affect the dynamics of the polymer segment in the domain under the NMR measurement conditions of this study. Further analysis focusing on the faster relaxation decay would provide more precise information for the HXDs. As seen in Fig. 6b, the larger $T_{2,3}$ value for PR06 than that for PR12 indicates that the network structure of the LXD of PR06 has a larger average mesh size than that of PR12, which results from the difference in the amount of cross-linker. The figure also shows that $T_{2,3}$ of PR06 and PR12 exhibits a steep decrease at the beginning of curing, which results from a decrease in the average molecular mobility of the polymer segments in the LXD.

Fig. 7a shows the change in the values φ_1, φ_2, and φ_3 as a function of the curing temperature. There is an insignificant change in each φ_i value for PR06 and PR12 over the temperature range of 115–130 °C, with the exception of a slight change at the beginning of the curing reaction from 110 to 115 °C. The smaller φ_2 value of 0.1–0.2 indicates that the structure defined as the interface region is a minor fraction in the network structure. Here, we introduce the parameter φ_{1+2}, which is the sum of φ_1 and φ_2, to simplify the structural model into two structures with a smaller T_2 of 10^0–10^1 ms and a larger T_2 of 10^2–10^3 ms because, although the interface region is necessary to explain the observed relaxation decay in the swollen state, the definition of the interface structure is ambiguous at present. The value φ_{1+2} represents the molar fraction of protons in the polymer segments whose molecular mobility is suppressed by the cross-links in the swollen state; therefore, this value could be related to the volume fraction of the HXDs in the dry state. The change in the value of φ_{1+2} as a function of the curing temperature is shown in Fig. 7b. The value φ_{1+2} for PR12 is larger than that for PR06 with an exception at 110 °C, which indicates that the dry-state volume fraction of the HXD in PR12 is larger than that in PR06, which would result from a stoichiometrically larger amount of cross-linker. Fig. 7b also shows that there is a slight but insignificant change in both the φ_{1+2} values for PR06 and PR12 over the temperature range of 115–130 °C. Here, the slight increase in φ_{1+2} indicates a slight increase in the size of the HXD in the dry state, while the absence of any significant change in φ_{1+2} indicates that the spatial location and size of the HXD in the dry state are determined at the beginning of the curing process and are essentially unchanged during the investigated temperature range. This conjecture could be explained by intradomain reactions being dominant in the initial curing process compared with interdomain reactions. It should be noted that the nature of the intradomain and interdomain reactions plays an important role in the growth of network structures of phenolic resins with cross-link inhomogeneity [14]. When the interdomain reaction between the HXD and LXD proceeds via the interface region, some part of the LXD is incorporated into the HXD accompanying an increase and a decrease in the number of protons in the HXD and LXD, respectively; hence, the interdomain reaction results in a distinct increase in the value φ_{1+2}. Conversely, the intradomain reaction in each

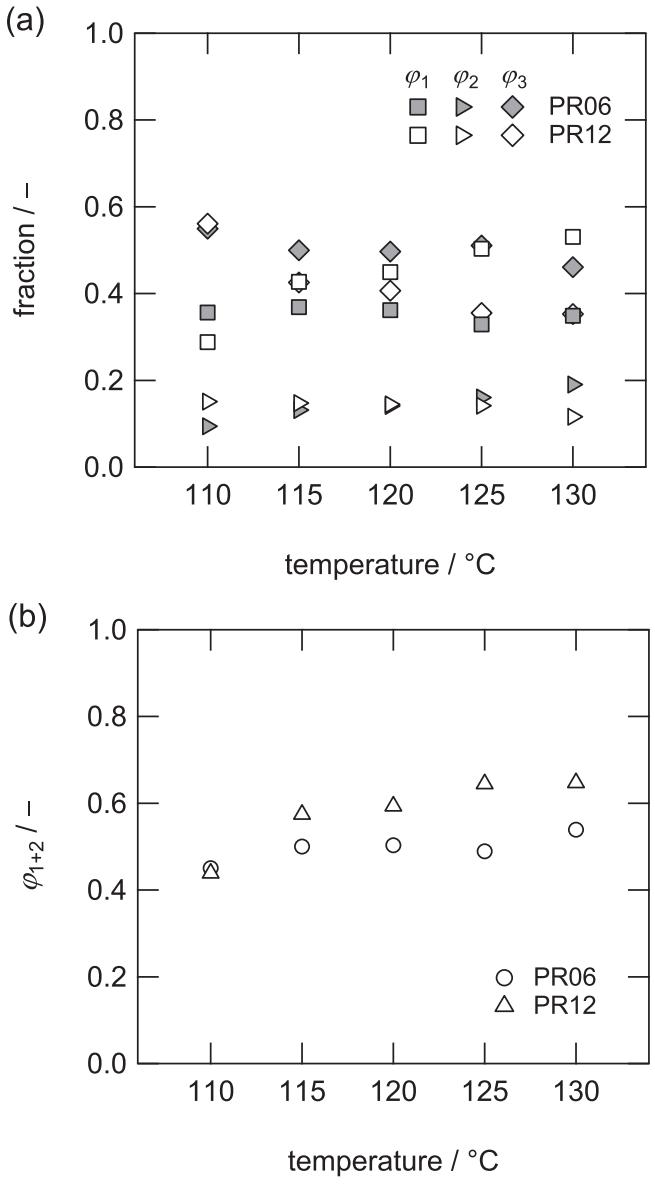

Fig. 7. (a) Changes in φ_1, φ_2, and φ_3 as a function of the curing temperature: squares, φ_1; right-pointing triangles, φ_2; diamonds, φ_3; filled symbols, PR06; and open symbols, PR12. (b) Change in φ_{1+2} as a function of curing temperature: circles, PR06; and triangles, PR12.

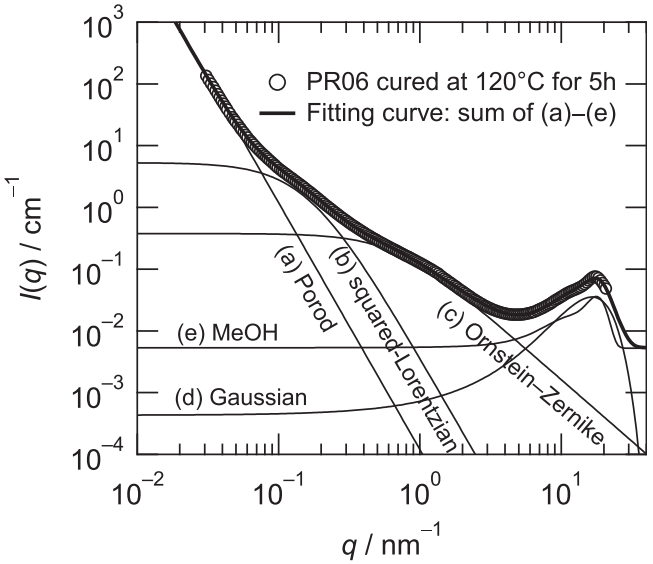

Fig. 8. Combined SAXS and WAXS curve for PR06 cured at 120 °C. Solid lines are fitting curves of Equation (4) and the five terms comprising the equation.

domain is a reaction between unreacted sites inside the domain, which leads to no significant structural change of the domain. Thus, the intradomain reaction results in no significant change in the time constant T_2, number of protons, spatial location, and volume of the domain. This accounts for the absence of significant change in the values of φ_{1+2} for PR06 and PR12 during the curing.

3.3. SAXS/WAXS

According to previous SAXS and SANS studies, small-angle scatterings from polymer gels can be explained by considering the solid-like cross-link inhomogeneity and the liquid-like concentration fluctuation of polymer chains [23–26,30]. The scattering functions of the inhomogeneity and the concentration fluctuation are generally represented by the squared-Lorentzian equation [33] ($I_{SL}(q)$) and the Ornstein–Zernike equation [34] ($I_{OZ}(q)$), respectively, and their combined scattering function has long been used to represent the structure of gels having cross-link inhomogeneity, which is given by

$$I(q) = \frac{I_{SL}(0)}{\left(1+\Xi^2 q^2\right)^2} + \frac{I_{OZ}(0)}{1+\xi^2 q^2}, \tag{3}$$

where $I(q)$, Ξ, and ξ denote the scattering intensity at q, and correlation lengths representing the characteristic size of inhomogeneity and that of the concentration fluctuation, respectively. Our previous studies demonstrated that this combined function is also applicable to phenolic resins when they are in the solvent swollen state [13,14]. For fully swollen phenolic resins, Ξ is related to the characteristic size of the inhomogeneity associated with the average sizes of the HXDs and LXDs, and ξ is related to the average mesh size of the LXD that behaves like a polymer chain in semidilute regime. It should be noted that this structural information for solvent swollen phenolic resins could be obtained in a small-angle scattering region with a q range of 10^{-2}–10^{0} nm^{-1}; however, a combination of SAXS and WAXS experiments over an extended q range of 10^{-2}–10^{1} nm^{-1} allows more precise analysis because the effect of X-ray scattering owing to the concentration fluctuation typically reaches a wide-angle scattering region of $q > 10^{0}$ nm^{-1} [13,14].

Fig. 8 shows the combined SAXS and WAXS curve for PR06 cured at 120 °C for 5 h, in which the curve was obtained in the fully MeOH-swollen state, and also includes solvent scattering. For curve fitting analysis over the wide q range of 0.03–20 nm^{-1}, three additional correction terms for Equation (3) were adopted; (i) surface scattering from MeOH-swollen gel particles with sizes larger than the micrometer scale or, more precisely, with sizes that can be observed below the experimental lower q limit, (ii) scattering from short-range electron density fluctuation of phenolic resins in the order of magnitude of 10^{-1} nm, and (iii) solvent scattering. The contribution of the terms (i) and (ii)–(iii) can be observed as scattering intensity upturns in the SAXS region of $q < 0.07$ nm^{-1} and in the WAXS region of $q > 6$ nm^{-1}, respectively. Thus, the theoretical scattering function of Equation (3) is revised to

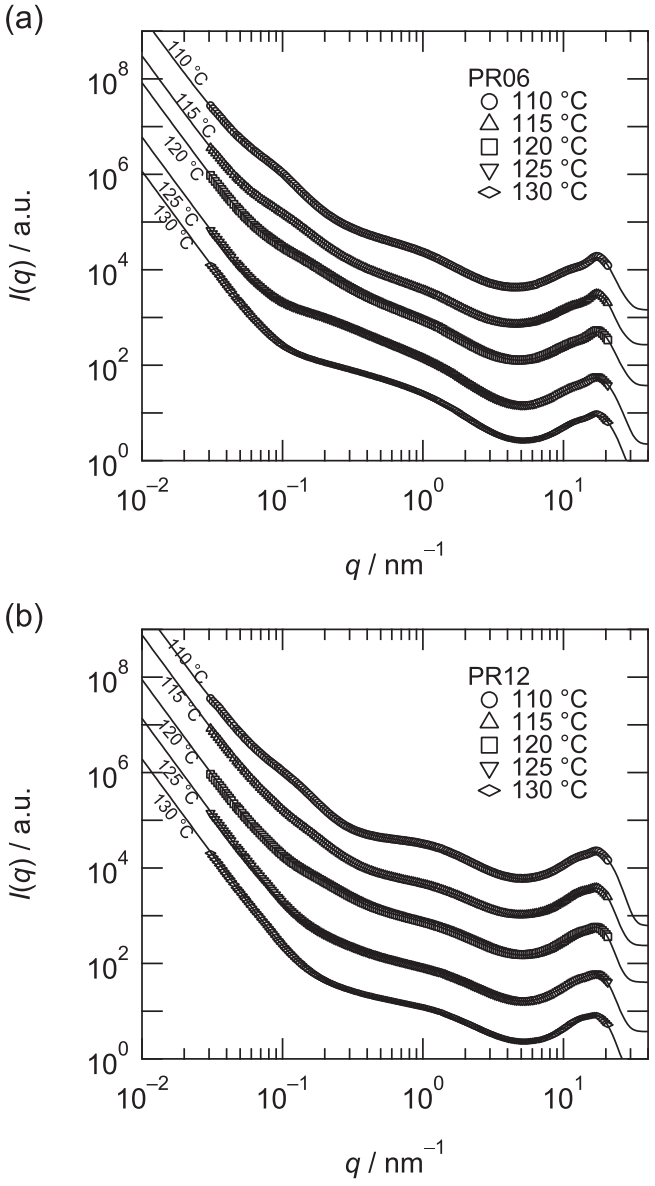

Fig. 9. Change in SAXS and WAXS curves as a function of curing temperature: (a) PR06 and PR12 in MeOH. Solid lines are fitting curves using Equation (4). The curves are arbitrarily vertically shifted to improve visibility.

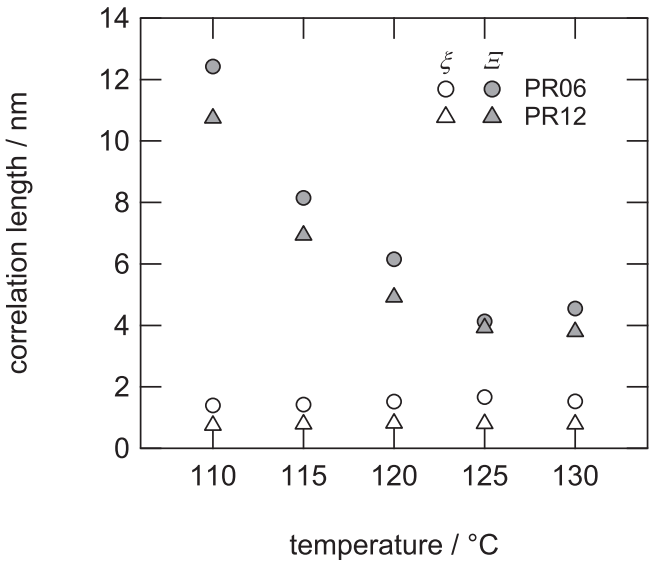

Fig. 10. Change in the fitting parameters of X-ray scattering curves as a function of curing temperature: circles, PR06; and triangles, PR12.

$$I(q) = A \cdot q^{-4} + \frac{I_{SL}(0)}{\left(1 + \Xi^2 q^2\right)^2} + \frac{I_{OZ}(0)}{1 + \xi^2 q^2} + B \cdot \exp\left(- \frac{(q - q_0)^2}{2w^2} \right) + C \cdot I_{MeOH}(q), \quad (4)$$

where A, B, and C represent scaling factors, q_0 and w denote peak position and width of a Gaussian function, respectively, and $I_{MeOH}(q)$ denotes the experimentally determined scattering function of MeOH. The first, fourth, and fifth terms on the right side of the equation correspond to the terms (i), (ii), and (iii), respectively, and the first term is known as Porod's law for flat-and-smooth surfaces [30]. The fitting curve using Equation (4) is shown in Fig. 8 by a solid line, and each of the five terms on the right of the equation is also represented in order to clarify their individual contribution to the scattering intensity. The results clearly show that Equation (4) accurately reproduces the observed X-ray scattering curve for the MeOH-swollen PR06 over the wide q range of 0.03–20 nm^{-1}.

Fig. 9a and b shows changes in the X-ray scattering curves for PR06 and PR12, respectively, in the fully-MeOH swollen state as a function of curing temperature. Solid lines are the fitting curves using Equation (4), which indicates the curve fitting is successful for all scattering data. Fig. 10 shows the change in the fitting parameters Ξ and ξ as a function of curing temperature. The results clearly show that both PR06 and PR12 exhibit almost the same values of Ξ and ξ at the respective temperature and curing proceeds with a decrease in Ξ while ξ remains constant, which indicates that the behavior of the network structure evolution with the cross-link inhomogeneity is essentially the same irrespective of the NV/HMTA-ratio.

The value of ξ being independent of the curing temperature indicates that the average mesh size of the LXD can be determined at the beginning of the curing, and remains unchanged during the initial curing process. The behavior of the values $T_{2,3}$ and ξ indicates that molecular mobility of the polymer segments in the LXD decreases without affecting the mesh size of the domain with increased curing temperature. This can be explained by considering that $T_{2,3}$ could be more significantly affected by polymer segments with very high molecular mobility, such as dangling chains in the domain; i.e., the steep decrease in $T_{2,3}$ as seen in Fig. 6b could result from intradomain reactions involving the dangling chains with very high molecular mobility, which would not significantly affect the average mesh size of the domain.

The decrease in Ξ with the curing process could be related to a decrease in the size of the LXD, because the progress of the gelation well beyond the gel point suggests that the HXD is dominant and the volume of the domain is sufficiently large. This conjecture and the behavior of φ_{1+2} indicate the presence of interdomain reactions between the HXDs. The reaction results in a slight but insignificant change in the number of protons both in the HXDs and LXDs; however, the reaction could result in a significant decrease in the size of the LXD in the solvent swollen state.

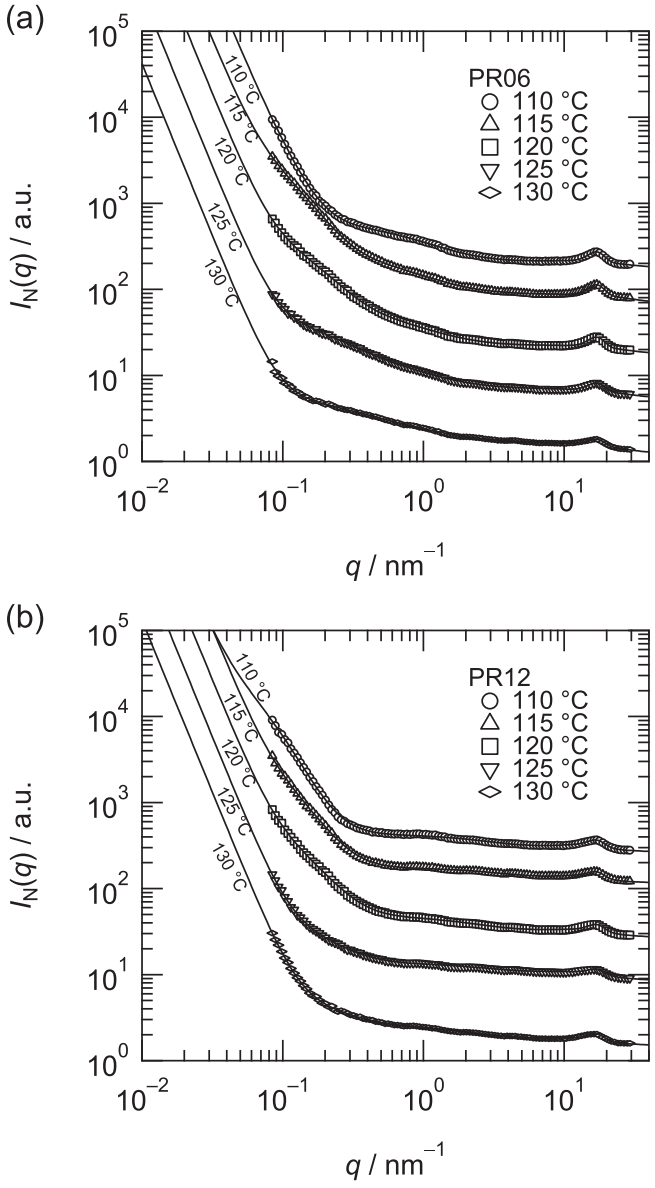

Fig. 11. Change in SANS and WANS curves as a function of curing temperature: (a) PR06 and PR12 in MeOH-d_4. Solid lines are fitting curves using Equation (5). The curves are arbitrarily vertically shifted to improve visibility.

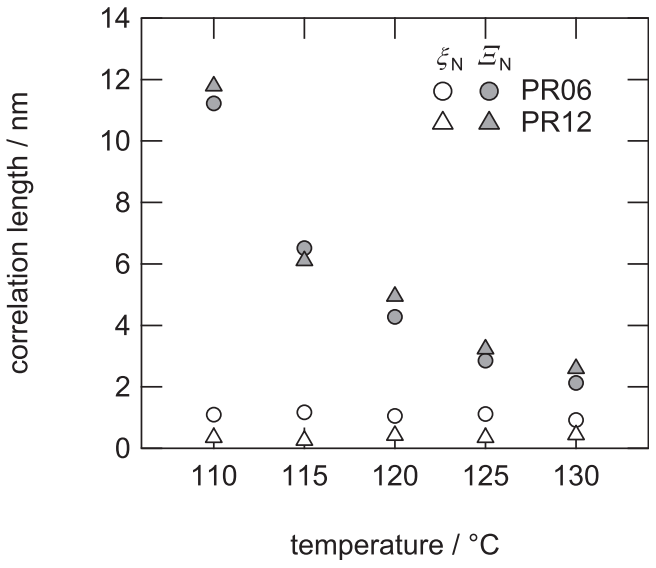

Fig. 12. Change in the fitting parameters of neutron scattering curves as a function of curing temperature: circles, PR06; and triangles, PR12.

3.4. SANS/WANS

To verify the results obtained using the X-ray scattering technique, complementary structural analysis was performed with fully MeOH-d_4-swollen phenolic resins using a combination of SANS and WANS measurements. The SANS and WANS results are shown in Fig. 11. The observed neutron scattering results from the same structural features of the solvent-swollen phenolic resins as observed by the X-ray scattering technique; therefore, the following theoretical scattering function based on Equation (4) was applied in the curve fitting analyses of the neutron scattering data over the wide q range of 0.08–30 nm^{-1}:

$$I_N(q) = A_N \cdot q^{-4} + \frac{I_{SL,N}(0)}{\left(1 + \Xi_N^2 q^2\right)^2} + \frac{I_{OZ,N}(0)}{1 + \xi_N^2 q^2} + B_N \cdot \exp\left(- \frac{\left(q - q_{0,N}\right)^2}{2w_N^2} \right) + C_N \cdot I_{MeOH-d_4}(q) + I_{incoh}, \quad (5)$$

where the definitions of the variables are the same as for Equation (4) (the subscript "$_N$" is added to distinguish them from those in Equation (4)), and I_{incoh} denotes incoherent neutron scattering background, which was approximated to be constant in the investigated q range. The fitting curves are shown by solid lines in Fig. 11, in which the cures accurately reflect the observed neutron scattering curve. Fig. 12 shows changes in the obtained fitting parameters Ξ_N and ξ_N as a function of curing temperature, which clearly supports the X-ray scattering results shown in Fig. 10.

3.5. Network structure evolution

Fig. 13 shows a schematic representation of the network structure evolution mechanism of phenolic resins, highlighting the interdependence of the stoichiometric amount of cross-linker and inhomogeneity in the initial stage of the curing. In the figure, the filled circles, thick circular outlines, and the spaces between them represent the HXD, the interface region, and the LXD, respectively, whose time constants are $T_{2,1}$, $T_{2,2}$, and $T_{2,3}$, respectively. Lines unconnected at one end represent dangling chains with a higher molecular mobility. The average distance between domain boundaries, which represents the characteristic size or degree of inhomogeneity, and the average mesh size of the LXD correspond to the correlation lengths Ξ and ξ, respectively.

The percolation of the HXDs occurs at 110 °C for both PR06 and PR12, in which the degree of cross-linking of the percolated domains dominates the degree of swelling of the gel. The HXD of PR12 has a tightly cross-linked, well-developed network structure from the beginning of the curing process, which results in a constant value of D_{swell} irrespective of the curing temperature. Conversely, PR06 has a more loosely cross-linked network structure compared with PR12, in which the degree of cross-linking in the domain increases via intradomain reactions accompanying a decrease in D_{swell} as curing progresses. The spatial location and size of the

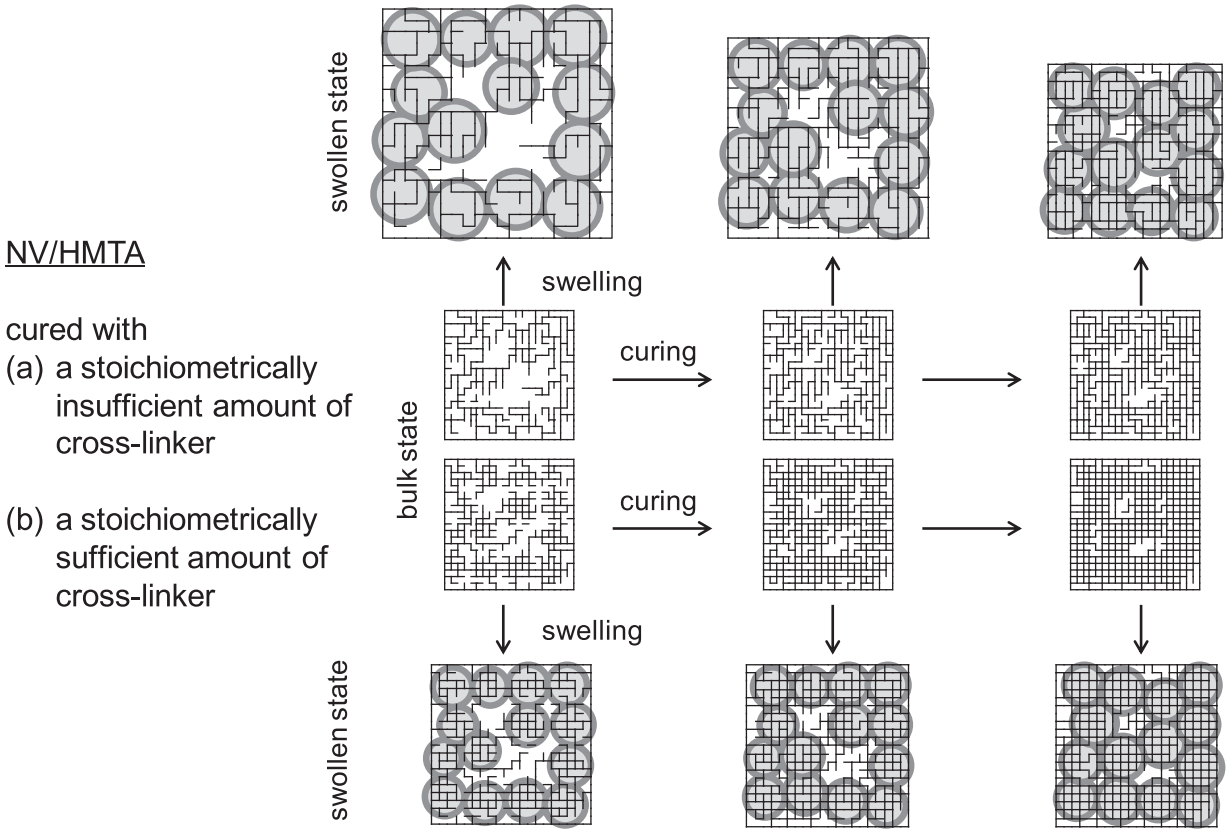

Fig. 13. Scheme of the network structure evolution mechanism representing the interdependence of the stoichiometric amount of cross-linker and the growth of the inhomogeneity of phenolic resins during the initial stage of the curing: (a) cured with a stoichiometrically insufficient amount of cross-linker, as in the case of PR06, and (b) cured with a stoichiometrically sufficient amount of cross-linker, as in the case of PR12. The filled circles, thick circular outlines, and the spaces between them represent the high-cross-link density, the interface, and the low-cross-link density regions, respectively, in the swollen state. Lines unconnected at one end represent dangling chains with a higher molecular mobility.

percolated domains in the dry state does not change significantly during the initial curing process because of the intradomain reactions being dominant for both HXDs and LXDs, which results in a slight but insignificant increase both in the φ_{1+2} values of PR06 and PR12 over the investigated temperature range. Conversely, the minor interdomain reaction at the interface between the HXDs results in a significant decrease in the size of the LXDs in the solvent swollen state, which results in the behavior of φ_{1+2} along with a decrease in Ξ. The intradomain reactions in the LXDs of PR06 and PR12 involved reactions with dangling chains with a very high molecular mobility, which does not affect the value of ξ significantly, but results in a steep decrease in $T_{2,3}$ at the beginning of the curing process owing to a decrease in the molecular mobility of the high mobility segments in the domain.

4. Conclusion

The cross-link inhomogeneity of phenolic resins at the initial stage of the curing process, well beyond the gel point, in a temperature range of 110–130 °C was successfully elucidated through structural analyses of the network structure evolution mechanism using ^{1}H-pulse NMR spectroscopy and the complementary SAXS/WAXS and SANS/WANS methods in conjunction with a solvent-swelling technique. Two types of phenolic resins PR06 and PR12 were prepared with stoichiometrically insufficient and sufficient amounts of cross-linker, respectively, via curing of NV with HMTA. Because of the cross-link inhomogeneity, their network structures comprised three different structures since the beginning of the curing process: HXD, LXD, and the interface region between HXD and LXD. The percolation of HXD occurred at the beginning of the curing. Intradomain reactions inside both HXD and LXD proceeded as the dominant reactions accompanying minor intrerdomain reactions between HXDs, which resulted in no significant change in the spatial location and size of the HXD and LXD. The intradomain reactions inside the LXD involve reactions with dangling chains, which would not significantly affect the average mesh size of the domain. These behaviors of the network structure evolution mechanism at the initial stage of curing are a general feature of phenolic resins that does not depend on the amount of cross-linker. The difference between the amount of cross-linker in PR06 and PR12 was manifested as the difference in the degree of cross-linking in the percolated HXDs, resulting in a difference in the degree of swelling, i.e., the HXD of PR12 exhibited a tightly cross-linked, well-developed network structure from the beginning of the curing process, whereas, the HXD of PR06 exhibited a loosely cross-linked network structure, with increasing degree of cross-linking as the curing proceeded.

We believe that this structural analysis method offers new insights for elucidating the inhomogeneity of cross-linked network structures in fully cured phenolic and other thermosetting resins, considering that a detailed clarification on this topic has not been provided in detail more than a century since the invention of the resins.

Acknowledgment

We would like to thank Hiroki Iwase of Research Center for Neutron Science and Technology, Comprehensive Research Organization for Science and Society (CROSS) and Shinichi Takata of J-PARC Center, Japan Atomic Energy Agency (JAEA) for helpful support in neutron scattering experiments. We would like to thank Jan Ilavsky of the Advanced Photon Source (APS) at Argonne National Laboratory for providing a glassy carbon plate and its SAXS data on the absolute intensity scale. We also would like to thank Asahi Kasei Corporation for providing the use of a vacuum sample chamber in the windowless SAXS measurement. The SAXS experiments were performed at the second hutch of SPring-8 BL03XU (Frontier Soft-material Beamline (FSBL)) constructed by the Consortium of Advanced Softmaterial Beamline with the proposal numbers of 2014A7201, 2014A7210, 2014A7211, 2014B7251, 2014B7260, and 2014B7261. The SANS/WANS experiments were performed at BL15 beamline in the Materials and Life Science Experimental Facility (MLF) of the J-PARC with the proposal number of 2014A0054. This study was conducted as a part of the research activities of the Special Interest Group on Thermosetting Resins in the FSBL Consortium comprising the Asahi Kasei research group (Terumasa Yamasaki, Kimio Imaizumi, Naoki Sakamoto, and Xiaobo Su of Asahi Kasei Corporation, Hisanao Yamamoto of Asahi Kasei E-Materials Corporation, Mitsukazu Ochi of Kansai Univ., and Shinichi Sakurai of Kyoto Institute of Technology), the DENSO research group (Akio Sugiura, Takashi Aoki, and Yasushi Okamoto of DENSO Corporation, Atsushi Takahara of Kyushu Univ., and Sono Sasaki of Kyoto Institute of Technology), and the Sumitomo Bakelite research group (the authors).

References

[1] A. Gardziella, L.A. Pilato, A. Knop, Phenolic Resins: Chemistry, Applications, Standardization, Safety and Ecology, 2nd, Springer, Berlin, 1999 completely rev.
[2] E. Venkatapathy, B. Laub, G.J. Hartman, J.O. Arnold, M.J. Wright, G.A. Allen, Thermal protection system development, testing, and qualification for atmospheric probes and sample return missions: examples for Saturn, Titan and Stardust-type sample return, Adv. Space Res. 44 (2009) 138–150.
[3] J.H. de Boer, The influence of van der Waals' forces and primary bonds on binding energy, strength and orientation, with special reference to some artificial resins, Trans. Faraday Soc. 32 (1936) 10–37.
[4] R. Houwink, The strength and modulus of elasticity of some amorphous materials, related to their internal structure, Trans. Faraday Soc. 32 (1936) 122–131.
[5] S.J. Bai, Crosslink distribution of epoxy networks studied by small-angle neutron-scattering, Polymer 26 (1985) 1053–1057.
[6] K. Dušek, Are cured thermoset resins inhomogeneous? Angew. Makromol. Chem. 240 (1996) 1–15.
[7] M.R. Vanlandingham, R.F. Eduljee, J.W. Gillespie, Relationships between stoichiometry, microstructure and properties for amine-cured epoxies, J. Appl. Polym. Sci. 71 (1999) 699–712.
[8] J.P. Pascault, H. Sautereau, J. Verdu, R.J.J. Williams, Thermosetting Polymers, Marcel Dekker, New York, 2002.
[9] J. Duchet, J.P. Pascault, Do epoxy-amine networks become inhomogeneous at the nanometric scale? J. Polym. Sci. Part B Polym. Phys. 41 (2003) 2422–2432.
[10] H. Kishi, T. Naitou, S. Matsuda, A. Murakami, Y. Muraji, Y. Nakagawa, Mechanical properties and inhomogeneous nanostructures of dicyandiamide-cured epoxy resins, J. Polym. Sci. Part B Polym. Phys. 45 (2007) 1425–1434.
[11] S. Morsch, Y. Liu, S.B. Lyon, S.R. Gibbon, Insights into epoxy network nanostructural heterogeneity using AFM-IR, ACS Appl. Mater. Interfaces 8 (2016) 959–966.
[12] A. Izumi, T. Takeuchi, T. Nakao, M. Shibayama, Dynamic light scattering and small-angle neutron scattering studies on phenolic resin solutions, Polymer 52 (2011) 4355–4361.
[13] A. Izumi, T. Nakao, M. Shibayama, Gelation and cross-link inhomogeneity of phenolic resins studied by ^{13}C-NMR spectroscopy and small-angle X-ray scattering, Soft Matter 9 (2013) 4188–4197.
[14] A. Izumi, T. Nakao, M. Shibayama, Gelation and cross-link inhomogeneity of phenolic resins studied by small- and wide-angle X-ray scattering and ^{1}H-pulse NMR spectroscopy, Polymer 59 (2015) 226–233.
[15] A. Izumi, T. Nakao, H. Iwase, M. Shibayama, Structural analysis of cured phenolic resins using complementary small-angle neutron and X-ray scattering and scanning electron microscopy, Soft Matter 8 (2012) 8438–8445.
[16] A. Izumi, T. Nakao, M. Shibayama, Synthesis and properties of a deuterated phenolic resin, J. Polym. Sci. Part A Polym. Chem. 49 (2011) 4941–4947.
[17] J.P. Cohen Addad, NMR and statistical structures of gels, in: J.P. Cohen Addad (Ed.), Physical Properties of Polymeric Gels, John Wiley, New York, 1996, pp. 39–86.
[18] R. Kimmich, N. Fatkullin, Polymer chain dynamics and NMR, Adv. Polym. Sci. 170 (2004) 1–113.
[19] A. Asano, NMR relaxation studies of elastomers, Annu. Rep. NMR Spectrosc. 86 (2015) 1–72.
[20] M. Nomoto, Y. Fujikawa, T. Komoto, T. Yamanobe, Structure and curing mechanism of high-ortho and random novolac resins as studied by NMR, J. Mol. Struct. 976 (2010) 419–426.
[21] K. Dušek, Diffusion control in the kinetics of cross-linking, Polym. Gels Netw. 4 (1996) 383–404.

[22] M. Shibayama, Spatial inhomogeneity and dynamic fluctuations of polymer gels, Macromol. Chem. Phys. 199 (1998) 1–30.
[23] M. Shibayama, Small-angle neutron scattering on polymer gels: phase behavior, inhomogeneities and deformation mechanisms, Polym. J. 43 (2011) 18–34.
[24] M. Shibayama, Structure-mechanical property relationship of tough hydrogels, Soft Matter 8 (2012) 8030–8038.
[25] W.L. Wu, M. Shibayama, S. Roy, H. Kurokawa, L.D. Coyne, S. Nomura, R.S. Stein, Physical gels of aqueous poly(vinyl alcohol) solutions: a small-angle neutron-scattering study, Macromolecules 23 (1990) 2245–2251.
[26] J. Bastide, S.J. Candau, Structure of gels as investigated by means of static scattering techniques, in: J.P. Cohen Addad (Ed.), Physical Properties of Polymeric Gels, John Wiley, New York, 1996, pp. 143–308.
[27] H. Masunaga, H. Ogawa, T. Takano, S. Sasaki, S. Goto, T. Tanaka, T. Seike, S. Takahashi, K. Takeshita, N. Nariyama, H. Ohashi, T. Ohata, Y. Furukawa, T. Matsushita, Y. Ishizawa, N. Yagi, M. Takata, H. Kitamura, K. Sakurai, K. Tashiro, A. Takahara, Y. Amamiya, K. Horie, M. Takenaka, T. Kanaya, H. Jinnai, H. Okuda, I. Akiba, I. Takahashi, K. Yamamoto, M. Hikosaka, S. Sakurai, Y. Shinohara, A. Okada, Y. Sugihara, Multipurpose soft-material SAXS/WAXS/GISAXS beamline at SPring-8, Polym. J. 43 (2011) 471–477.
[28] A. Takahara, T. Takeda, T. Kanaya, N. Kido, K. Sakurai, H. Masunaga, H. Ogawa, M. Takata, Advanced soft material beamline consortium at SPring-8 (FSBL), Synchrotron Radiat. News 27 (2014) 19–23.
[29] F. Zhang, J. Ilavsky, G.G. Long, J.P.G. Quintana, A.J. Allen, P.R. Jemian, Glassy carbon as an absolute intensity calibration standard for small-angle scattering, Metall. Mater. Trans. A 41A (2010) 1151–1158.
[30] R.J. Roe, Methods of X-ray and Neutron Scattering in Polymer Science, Oxford University Press, New York, 2000.
[31] S. Takata, J. Suzuki, T. Shinohara, T. Oku, T. Tominaga, K. Ohishi, H. Iwase, T. Nakatani, Y. Inamura, T. Ito, K. Suzuya, K. Aizawa, M. Arai, T. Otomo, M. Sugiyama, The design and q resolution of the small and wide angle neutron scattering instrument (TAIKAN) in J-PARC, JPS Conf. Proc. 8 (2015) 036020.
[32] T. Canal, N.A. Peppas, Correlation between mesh size and equilibrium degree of swelling of polymeric networks, J. Biomed. Mater. Res. 23 (1989) 1183–1193.
[33] P. Debye, A.M. Bueche, Scattering by an inhomogeneous solid, J. Appl. Phys. 20 (1949) 518–525.
[34] H.E. Stanley, Introduction to Phase Transitions and Critical Phenomena, Oxford University Press, New York, 1971.